Journal of Science: Advanced Materials and Devices 1 (2016) 512–520

Contents lists available at ScienceDirect

Journal of Science: Advanced Materials and Devices

journal homepage: www.elsevier.com/locate/jsamd

Original Article

Transport phenomena and conductivity mechanism in Sm doped $Bi_4V_{2-x}Sm_xO_{11}$ ceramics

Sasmitarani Bag, Banarji Behera*

Material Research Laboratory, School of Physics, Sambalpur University, Jyoti Vihar, Burla, Odisha, 768 019, India

ARTICLE INFO

Article history:
Received 24 August 2016
Accepted 12 October 2016
Available online 18 October 2016

Keywords:
Aurivillius
Solid-state reaction
Impedance
Electrical conductivity
Activation energy

ABSTRACT

The polycrystalline samples of Sm doped $Bi_4V_{2-x}Sm_xO_{11}$ with x = 0.05, 0.10, 0.15 and 0.20 ceramics were prepared by using solid-state reaction technique. The structural characterization of the prepared samples were confirmed by X-ray powder diffraction (XRD) and showed an orthorhombic and monoclinic phase. The nature of Nyquist plot confirms the presence of both grain and grain boundary effects for all Sm doped compounds. The grain resistance decreases with rise in temperature for all the samples and exhibits a typical negative temperature co-efficient of resistance (NTCR) behavior. The ac conductivity spectrum obeys Jonscher's universal power law. The modulus analysis suggests a possible hopping mechanism for electrical transport processes of the materials. The nature of variation of dc conductivity suggests the Arrhenius type of electrical conductivity for all the samples.

1. Introduction

Recently, a lot of research has been carried out on the Bismuth Layered Structured Ferroelectric (BLSF) materials of the Aurivillius family, first studied by Aurivillius [1] in 1950 having the general formula $(Bi_2O_2)^{2+}$ $(A_{m-1}B_mO_{3m+1})^{2-}$, which consists of m-perovskite unit sandwiched between bismuth oxide layers called the family of BLSFs, where A and B are the two types of cation that enter the perovskite unit (A is Bi^{3+}, Ba^{2+}, Sr^{2+}, Pb^{2+}or K^{1+} and B is Ti^{4+}, Ta^{5+}, Nb^{5+}, Mo^{6+} or W^{6+} and m = 1, 2, 3, 4, 5, 6). The crystal structure is built up of two perovskites-like layers, infinite in two dimensions and alternating with a layer of $(Bi_2O_2)^{2+}$ along the c-axis.

Bismuth Vanadate $Bi_4V_2O_{11}$ is a group of the Aurivillius family having general formula $(Bi_2O_2)^{2+}$ $(A_{m-1}B_mO_{3m+1})^{2-}$ with m = 1. It consists of layer of $(Bi_2O_2)^{2+}$ interleaved with the perovskite-like sheets of V_2O_5 with the perovskite slab containing oxygen vacancies and responsible for the high ionic conductivity of oxides [2,3]. These materials are used for various applications such as catalyst properties, gas sensors, solid state electrolytes as electrode materials for lithium rechargeable batteries, pyroelectric detectors, fuel cells, oxygen pumps, space and land based pulsed power application etc [3–5]. Much research work has been reported in the literature aimed to improve the electrical properties of such materials. $Bi_4V_2O_{11}$ compound has three modified structure in the form of α, β and γ. These are mainly due to two structure form: α (monoclinic and orthorhombic) phase and stable in the room temperature (RT) to 440 °C, β (orthorhombic) phase and stable in the temperature range (440 °C–560 °C) and the γ (tetragonal) phase which is found beyond 560 °C [6]. The microstructures of BIMEVOXes and the ME doped materials (Ni, Co, Cu, Zn) are studied using impedance synthesis [7]. Politova et al. studied both A and B site doped samples of $(Bi_{1-y}La_y)_4$ $(V_{1-x}Me_x)_2O_{11-y}$ with x, y < 0.2, Me = Zr, Ga, Fe, Ca [8]. Morozova et al. studied, using three different methods (conventional solid state synthesis, mechanical activation and liquid precursors), to prepare the vanadium doped samples $Bi_4V_{2-x}Cu_{x/2}Ti_{x/2}O_{11-x}$ $(0.025 \le x \le 0.5)$ [9]. Szreder et al. studied the linear and non linear ac conductivity as a function of frequency, temperature and ac voltage [10]. Sei-Ki Kim et al. studied the Co doped at the B site of $Bi_4V_{2-x}Co_xO_{11-\delta}$ and confirmed a high anisotropy of the ionic conductivity between the directions of both parallel and perpendicular to $(Bi_2O_2)^{2+}$ layer [11]. Gupta et al. studied the Barium doped $Bi_4Ba_xV_{2-x}O_{11-\delta}$ $(0.0 \le x \le 0.15)$ using melt quench technique [12]. Ravi Kant et al. also studied the Ti doped $Bi_4V_{2-x}Ti_xO_{11-\delta}$ $(0 \le x \le 0.4)$ [13]. Politova et al. studied the dielectric conductivity and impedance properties of $(Bi_{1-y}La_y)_4(V_{1-x}Zr_x)_2O_{11-y}$ with x = 0–0.05, y = 0–0.16 and confirmed the influence of both intrinsic oxygen vacancies and 'Pinned' at ferroelectric domain boundaries on the temperature

* Corresponding author.
E-mail address: banarjibehera@gmail.com (B. Behera).
Peer review under responsibility of Vietnam National University, Hanoi.

http://dx.doi.org/10.1016/j.jsamd.2016.10.004

dependence hysteresis of α and β phase transition [14]. Torba et al. studied (100-n) $Bi_4V_2O_{11-z}$ − n $Ce_{0.9}Gd_{0.1}O_{1.9}$ with n = 0÷25 wt% [15]. Thakur et al. studied the structural and optical properties of La and Gd doping $Bi_{4-x}M_xV_2O_{11-\delta}$ ($0.1 \leq x \leq 0.3$) [16]. Gupta et al. again studied $Bi_4V_{2-x}Mg_xO_{11-\delta}$ (x = 0.05, 0.10 and 0.20) and $Bi_4V_{2-x}Ca_xO_{11-\delta}$ (x = 0.05, 0.10, 0.15 and 0.20) [17]. Yasuda et al. studied the impedance analysis on electrical anisotropy of layer-structured $Bi_4V_{2(1-x)}Co_{2x}O_{11-\delta}$ single crystals [18]. Khaerudini et al. studied the Nb doped $Bi_4V_{2-x}Nb_xO_{11-\delta}$ and reported three structurally related phase changes that effect of vacancy order/disorder over the oxygen atom positions [19]. The values of two component of complex impedance and the relaxation time of oxide ion movement through the grain interior and grain boundary decreases with increase in temperature of $Bi_2V_{0.9}Co_{0.1-x}Ti_xO_{5.35+x}$ ($0.02 \leq x \leq 0.08$) was studied by Beg et al. [20]. Many authors have reported the analysis of different materials using impedance spectroscopy [21,22]. We have, recently, reported on the structural, dielectric and ferroelectric properties of layered bismuth oxide of Sm doped $Bi_4V_{2-x}Sm_xO_{11}$ (x = 0.00, 0.05, 0.10, 0.15 and 0.20) ceramics [23]. The present paper reports the transport properties of layered bismuth oxide structure compounds of Sm doped $Bi_4V_{2-x}Sm_xO_{11}$ (x = 0.05, 0.10, 0.15 and 0.20).

2. Experimental

The polycrystalline samples of samarium doped $Bi_4V_{2-x}Sm_xO_{11}$ with x = 0.05, 0.10, 0.15 and 0.20 were prepared using solid state reaction method by taking high purity ingredients; Bi_2O_3 (99%), Sm_2O_3 (99.9%), V_2O_5 (98.5%) in a suitable stoichiometry. The stoichiometric amount of weighed compositions were mixed thoroughly; first in an air atmosphere for 1 h and then in alcohol for 2 h. Then mixed powders were calcined in a high purity alumina crucible at an optimized temperature of 700 °C for 3 h in an air atmosphere. The formations of the compounds were checked by X-ray diffraction technique (XRD) at room temperature. Then the fine homogenous powder was cold pressed into cylindrical pellets of 12 mm diameter and 1–2 mm of thickness at pressure of 4×10^6 Pa using a hydraulic press. These pellets were sintered at 750 °C for 3 h in an air atmosphere. Finally, the sintered pellets were polished with fine emery paper to make both the surfaces smooth and parallel. The pellets were coated with high purity silver paste and dried at temperature 150 °C for electrical measurements. The impedance parameters were obtained using a computer controlled LCR meter (HIOKI Model 3532) in a wide frequency range (10^2–10^6 Hz) at different temperatures (25–450 °C).

3. Results and discussion

3.1. Structural study

Room temperature XRD pattern (Fig. 1) of fine homogenous calcined powders for all Sm compositions of $Bi_4V_{2-x}Sm_xO_{11}$ (x = 0.05, 0.10, 0.15 and 0.20) were taken and confirmed an orthorhombic and monoclinic crystal structures. It is observed that, for x = 0.05–0.10 samples exhibit characteristic doublet at $2\theta \approx 32°$ and singlet at $2\theta \approx 46°$, which suggests the β phase orthorhombic crystal structure [24] and for x = 0.15–0.20 samples exhibit characteristic both are doublet at $2\theta \approx 32°$ and 46°, which suggests the α phase monoclinic crystal structure [25] at room temperature. A good agreement between observed (obs) and calculated (cal) interplanar spacing d ($\sum\Delta d = d_{obs} - d_{cal} =$ minimum) was observed. The values of the lattice parameters shown in Table 1 and were evaluated by using a standard computer program package "POWD" [26] for all Sm concentration. The crystallite size (P) of Sm doped samples were roughly estimated from the broadening of a few XRD peaks (in a wide 2θ range) using the Scherrer's equation [27], $P = K\lambda\left(\beta_{\frac{1}{2}} \cos\theta_{hkl}\right)$ (where K = constant = 0.89, λ = 1.5405 Å and $\beta_{1/2}$ = peak width of the reflection at half intensity). The average values of P were found to be 30–55 nm.

3.2. Impedance study

The complex impedance spectroscopy (CIS) [28] is a unique and powerful technique to analyze the electrical response (i.e., transport properties). Generally, the contribution of grain, grain boundary and electrode effect of polycrystalline samples in a

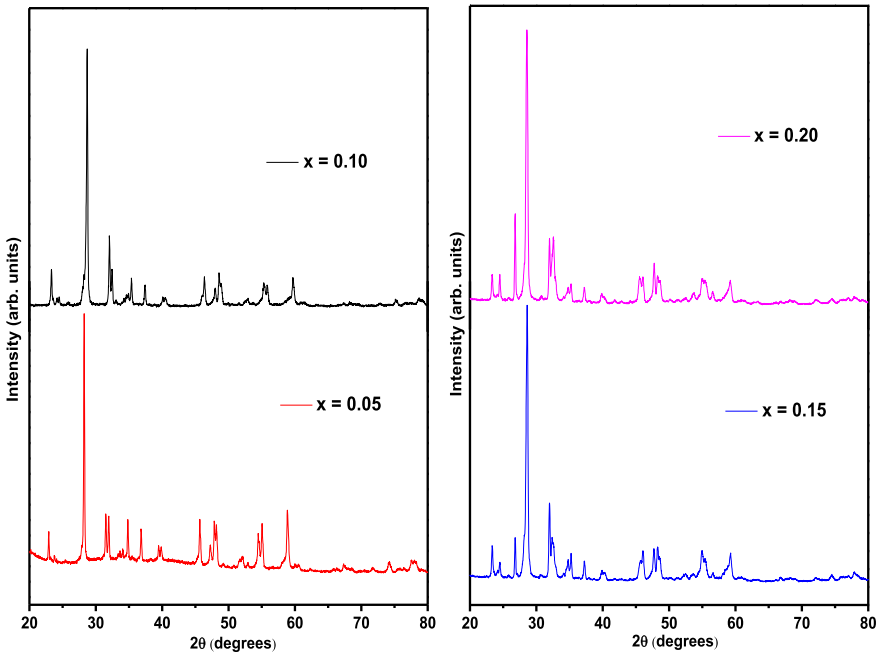

Fig. 1. XRD pattern of $Bi_4V_{2-x}Sm_xO_{11}$ for x = 0.05, 0.10, 0.15 and 0.20 at room temperature.

Table 1
Values of lattice parameters of $Bi_4V_{2-x}Sm_xO_{11}$ (x = 0.05, 0.10, 0.15 and 0.20).

x	a (Å)	b (Å)	c (Å)	V (Å^3)	Structure
0.05	5.562	5.608	15.387	479.96	Orthorhombic
0.10	5.561	5.611	15.338	478.59	Orthorhombic
0.15	5.541	5.618	15.344	477.61	Monoclinic
0.20	5.544	5.617	15.355	478.165	Monoclinic

wide range of frequency at different temperatures cause analyzed. The electrical properties of a material is often represented in terms of complex dielectric constant (ε^*), complex impedance (Z^*), electric modulus (M^*) and loss tangent ($\tan\delta$). These are related to each other as *i)* $Z^* = Z' - jZ'' = R - \frac{1}{j\omega C}$ *ii)* $M^* = \frac{1}{\varepsilon^*(\omega)} = M' + jM'' = j\omega C_0 Z^*$ *iii)* $\varepsilon^* = \varepsilon' - j\varepsilon''$ *iv)* $\tan\delta = \frac{\varepsilon''}{\varepsilon'} = \frac{M''}{M'} = \frac{Z'}{Z''}$, where (Z′, M′, ε′) and (Z″, M″, ε″) are real and imaginary components of impedance, modulus and permittivity, j = $\sqrt{-1}$ the imaginary factor, C_o = vacuum capacitance. A complex impedance spectrum of ceramic sample shows two distinct features intragrain (grain) and intergrain (grain boundary). Impedance data are presented in the form of Z″ (Capacitive) and Z′ (resistive). The complex impedance of the electrode/ceramic/electrode configuration can be explained as the sum of a single RC (R = Resistance and C = capacitance) circuit in parallel combination.

Fig. 2(a–d) shows the complex impedance spectrum (Z′ vs Z″) of $Bi_4V_{2-x}Sm_xO_{11}$ with x = 0.05, 0.10, 0.15 and 0.20 at different temperatures (275–350 °C). Generally, the impedance properties arise due to the grain, grain boundary and electrode processes. In the Nyquist plots, both the grain and grain boundary effects are present for all the compositions. The semicircles are found to be depressed with their centers lying below the real axis, which confirms the existence of non-Debye type relaxation phenomena. It is also confirmed the presence of grain and grain boundary effects in the materials with the increase in the percentage of Sm concentration. A similar type of behavior is also observed in other bismuth layered structured compounds [19,29]. From the complex impedance spectrum, it is found that the grain and grain boundary resistance decreases with rise in temperature which shows the negative temperature coefficient resistance (NTCR) behavior of the compounds like a semiconductor. The electrical process taking place within the materials can be model (as an RC circuit) on the basis of the brick-layer model [25]. The impedance data are fitted with the ZsimpWin software with an equivalent circuits (shown in inset of Fig. 2(a–d)) at 350 °C of $Bi_4V_{2-x}Sm_xO_{11}$ with x = 0.05, 0.10, 0.15 and 0.20. The values of fitting parameters of the circuits are shown in the Table 2.

Fig. 3(a–d) shows the variation of real part of the impedance (Z′) with frequency at different temperatures (275–350 °C) of $Bi_4V_{2-x}Sm_xO_{11}$ with x = 0.05, 0.10, 0.15 and 0.20. It is observed that the magnitude of Z′ (grain resistance) decreases with rise in temperature as well as Sm concentration in the low frequency range, and thereafter, appears to merge in the high frequency region. This may be due to the release of space charge polarization with rise in temperature and frequency [30]. This behavior indicates that the conduction mechanism increases with rise in temperature (i.e., NTCR behavior like a semiconductor). The space charge

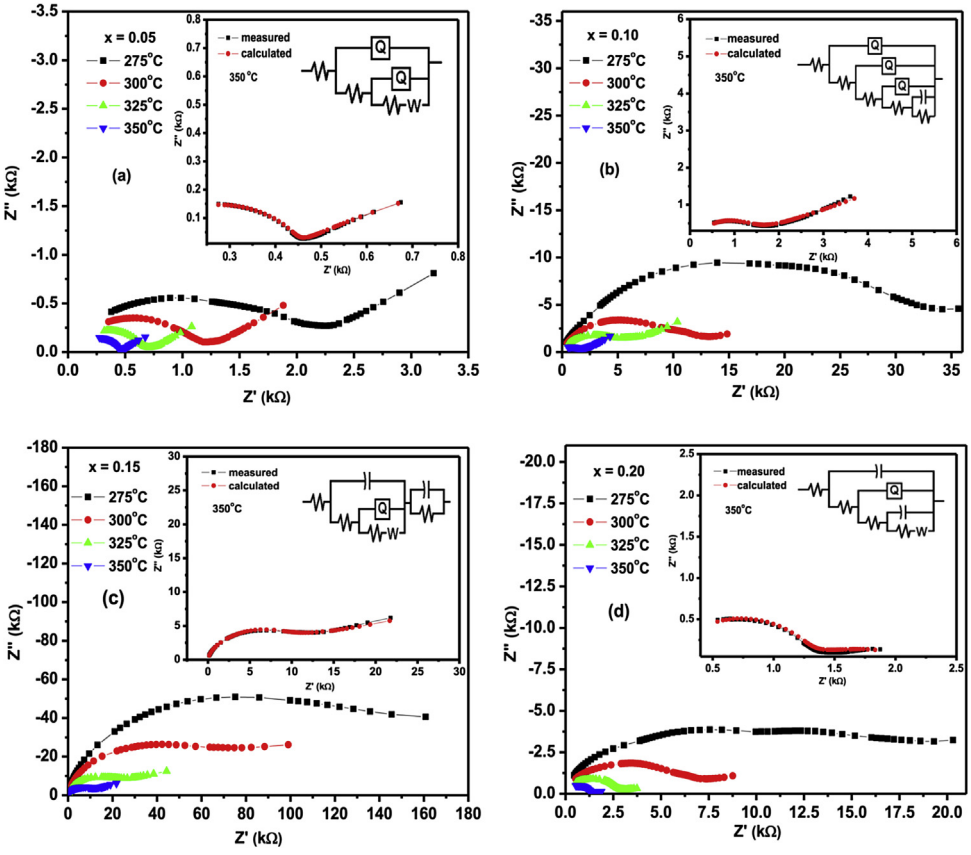

Fig. 2. Complex impedance spectrum (Z′ vs Z″) with equivalent circuit (inset) of $Bi_4V_{2-x}Sm_xO_{11}$ for x = 0.05, 0.10, 0.15 and 0.20 at different temperatures.

Table 2
Values of fitting parameters of the equivalent circuits of $Bi_4V_{2-x}Sm_xO_{11}$ with x = 0.05, 0.10, 0.15 and 0.20 at 350 °C.

Different parameters	x = 0.05	x = 0.10	x = 0.15	x = 0.20
R_1	97.46	134.4	44.98	200.2
R_2	342.1	897.8	0.004685	942.2
R_3	1910	8.651×10^{13}	6.196	5.879
R_4		167.4	226.5	1091
R_5		1.797×10^{13}		
C_1		2.392×10^{-8}	2.388×10^{-10}	2.144×10^{-10}
C_2			2.590×10^{-9}	8.904×10^{-10}
CPE (Q_1)	2.302×10^{-9}	8.105×10^{-10}	1.608×10^{-5}	8.743×10^{-5}
Q_2	20310	4.794×10^{-5}		
Q_3		1.956×10^{-8}		
Frequency power (n_1)	0.8944	0.9031	0.1685	
n_2	0.4286	0.261		
n_3		0.02628		
Chi square	4.578×10^{-5}	5.422×10^{-4}	1.453×10^{-4}	5.268×10^{-4}
Warburg	1.381×10^{11}		8.220×10^{-8}	2.666×10^{15}

polarization occurs maximum at higher frequency side for x = 0.05 as compared to other concentrations. This may be due to the Sm doped on vanadium sites and reduction in barrier properties with rise in temperature and responsible for the enhancement of conductivity of the materials [31,32]. Similar type of behavior also observed in other studied material [33]. It is also observed the value of Z′ increases with increase in Sm concentration up to x = 0.05–0.15 and then decreases.

Fig. 4(a–d) shows the frequency-temperature dependence of Z″ (usually called as loss spectrum) of $Bi_4V_{2-x}Sm_xO_{11}$ with x = 0.05, 0.10, 0.15 and 0.20. The magnitude of Z″ decreases with increase in frequency as well as with temperature for all the concentration. The appearance of peaks in the loss spectrum suggests the existence of relaxation process and shift towards the high frequency side for all the concentrations. This may due to the immobile species at low temperatures and defect or vacancies at high temperatures [34]. At high frequency, it is clear that there is an absence of space charge effect in the materials.

3.3. Modulus study

The complex modulus spectroscopy is a very convenient tool to analyze the dynamical aspects of electrical transport phenomena in the materials. The complex electrical impedance spectrum gives more emphasis to elements with large resistance whereas complex electric modulus spectrum plots highlight those with smaller

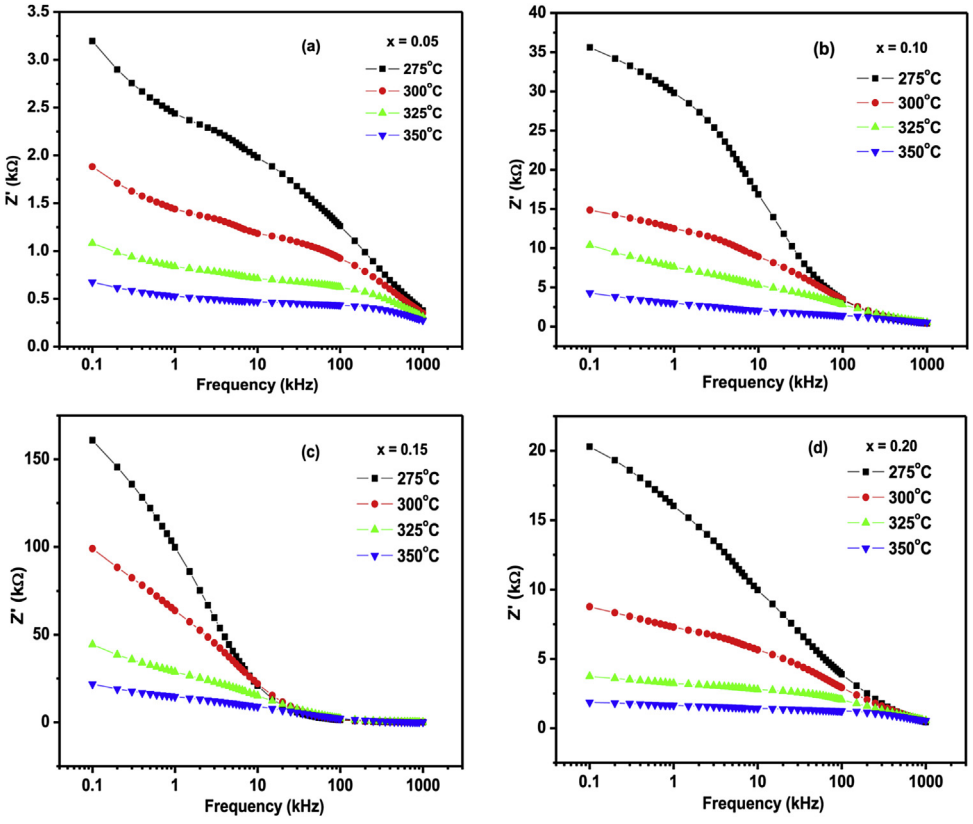

Fig. 3. Variation of Z′ with frequency of $Bi_4V_{2-x}Sm_xO_{11}$ for x = 0.05, 0.10, 0.15 and 0.20 at different temperatures.

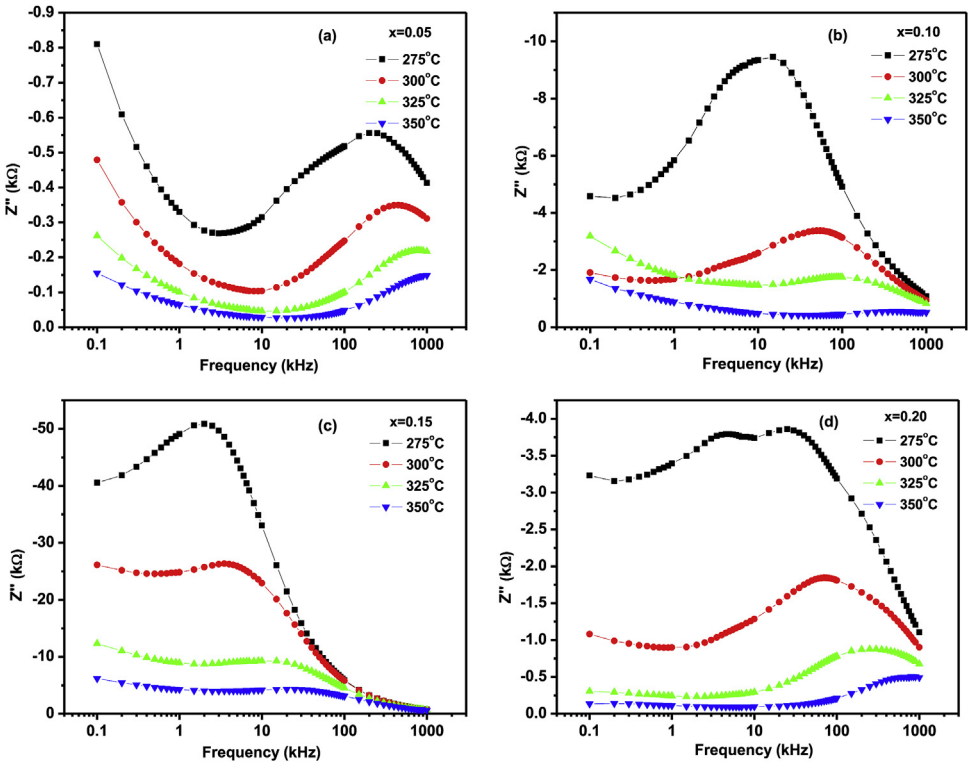

Fig. 4. Variation of Z″ with frequency of $Bi_4V_{2-x}Sm_xO_{11}$ for x = 0.05, 0.10, 0.15 and 0.20 at different temperatures.

capacitance. Using the complex modulus formula, the inhomogeneous nature of the polycrystalline compounds with grain and grain boundary effects can be probed easily, which cannot be distinguished from complex impedance plots and the other advantage of the electric modulus spectrum formulae is the suppressed of electrode effect. The real and imaginary components of the complex electric modulus (M*) were calculated by using the relation $M' = \omega C_0 Z''$, $M'' = \omega C_0 Z'$ ($\omega = 2\pi f_r$, $C_0 = \varepsilon_0 A/t$), where ω, C_0, ε_0, A, t and f_r are the angular frequency, geometrical capacitance, permittivity of free space, area of the electrode surface, thickness and relaxation frequency.

Fig. 5(a–d) shows the variation of M′ as a function of frequency of $Bi_4V_{2-x}Sm_xO_{11}$ with x = 0.05, 0.10, 0.15 and 0.20 at different temperatures (275–350 °C). For all the concentrations, it shows that a very low value (approximately zero) of M′ in the low frequency region. A continuous dispersion on increasing frequency and saturation at a maximum asymptotic value (i.e., M_∞) in the higher frequency region were observed for all the temperatures (275–350 °C). It may possibly be related to a lack of restoring force governing the mobility of the charge carriers under the action of an induced electrical field. The value of M′ decreases with rise in temperature in the high frequency region for all the concentrations. Similar type of behavior also observed in other reported material [35,36].

Fig. 6(a–d) shows the variation of imaginary part of electric modulus (M″) with frequency of $Bi_4V_{2-x}Sm_xO_{11}$ with x = 0.05, 0.10, 0.15 and 0.20 at different temperatures (275–350 °C). A well-defined relaxation mechanism is observed for the concentration x = 0.10–0.20 expect x = 0.05 at different temperatures. The relaxation peaks shift towards higher frequency side with rise in temperature which correlates between motion of mobile ions [37]. This suggests that the relaxation is thermally activated process. The asymmetry of peak broadening shows the spread of relaxation times with different time constant. Hence, it shows relaxation is of non-Debye type. The maximum value of M″ increases with rising temperatures (275–325 °C) and no peaks are observed for the concentration x = 0.10 and 0.20 at ≥350 °C. This may be due to the limitation on our measurements (i.e., 10^2–10^6 Hz). The maximum modulus peaks (M''_{Max}) are observed for x = 0.10–0.20. Similar type of behavior also observed in other reported material [35].

Fig. 7(a–d) shows the complex modulus spectrum (M′ vs M″) of $Bi_4V_{2-x}Sm_xO_{11}$ with x = 0.05, 0.10, 0.15 and 0.20 at different temperatures. The impedance data were again re-plotted in the modulus formula. This clearly indicates that a semicircle is formed for all the concentrations. This also confirms the presence of electrical relaxation phenomena in the materials. On increasing temperature, the intercept on real axis shifts towards the higher value of M′. This indicates the increase in capacitance of the materials. The intercept point on the real axis indicates that the grain effect contributes the total capacitance. It also supports the negative temperature Coefficient of resistance type behavior of the materials since grain capacitance (C_g) is inversely proportional to the grain resistance (R_g). Similar type of results also observed in other reported material [36,38].

4. Electrical conductivity study

Fig. 8(a–d) shows the ac electrical conductivity as a function of frequency of $Bi_4V_{2-x}Sm_xO_{11}$ with x = 0.05, 0.10, 0.15 and 0.20 at different temperatures (275–350 °C). The conductivity is well described by Jonscher's universal power law [39],$\sigma(\omega) = \sigma_0 + A\omega^n$, where σ_o is a dc conductivity in particular range of temperature, A is a temperature dependent parameter, $A\omega^n$ consisting of the ac dependence and characterizes for all dispersion phenomena and the exponent 'n' is the temperature

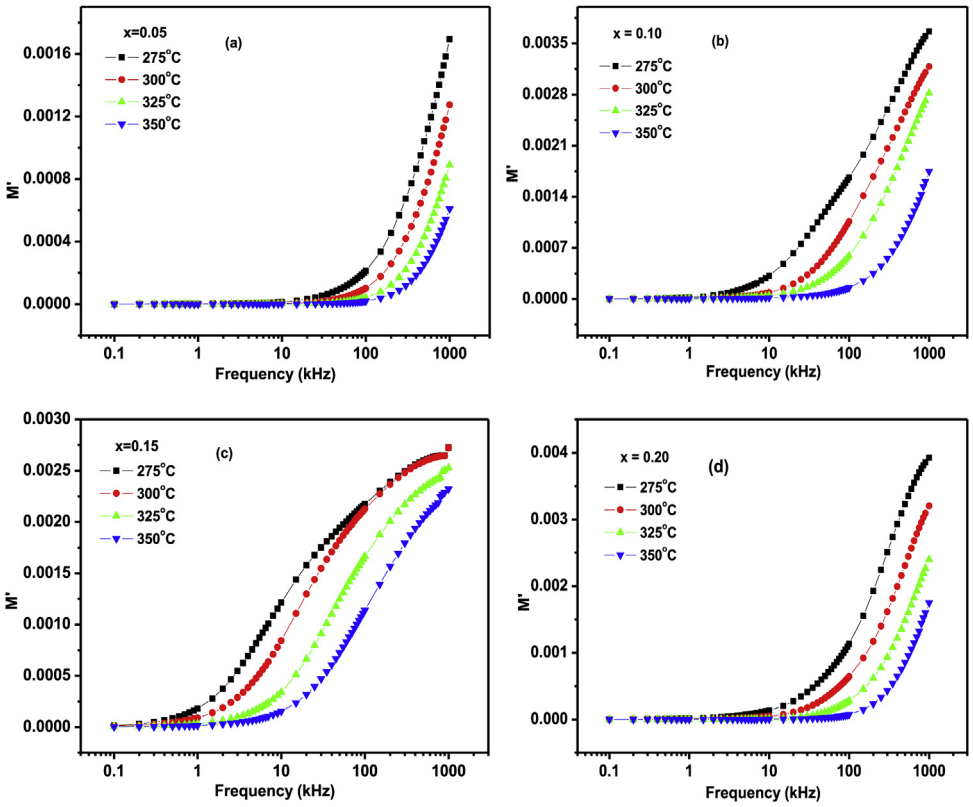

Fig. 5. Variation of M′ as a function of frequency of $Bi_4V_{2-x}Sm_xO_{11}$ for x = 0.05, 0.10, 0.15 and 0.20 at different temperatures.

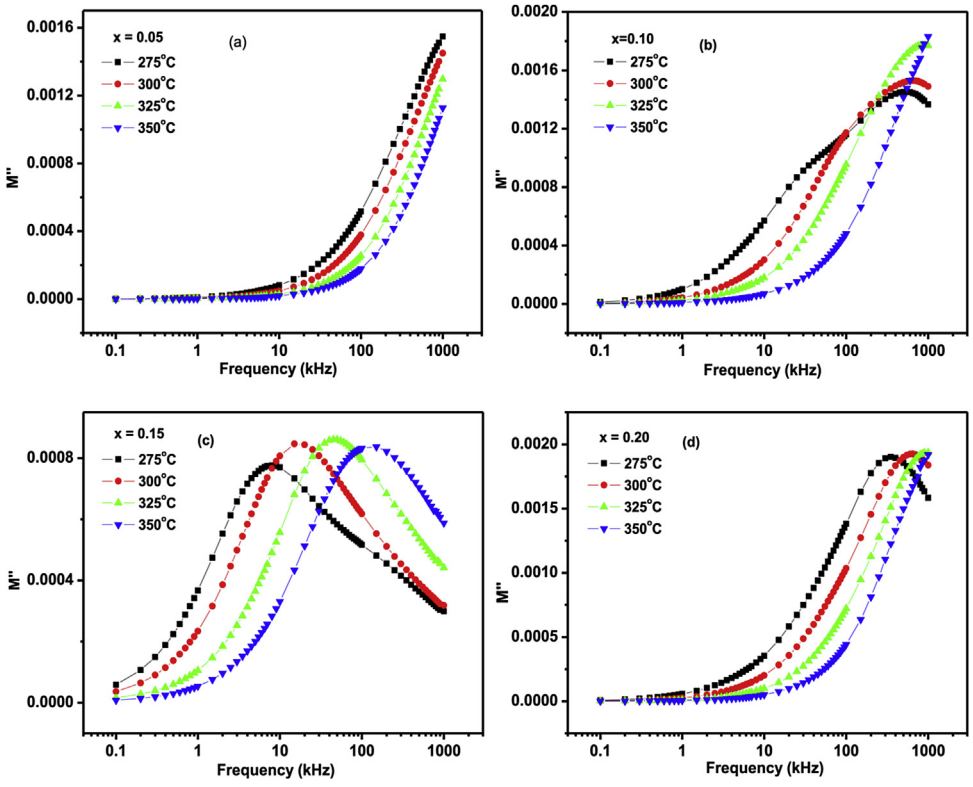

Fig. 6. Variation of M″ as a function of frequency of $Bi_4V_{2-x}Sm_xO_{11}$ for x = 0.05, 0.10, 0.15 and 0.20 at different temperatures.

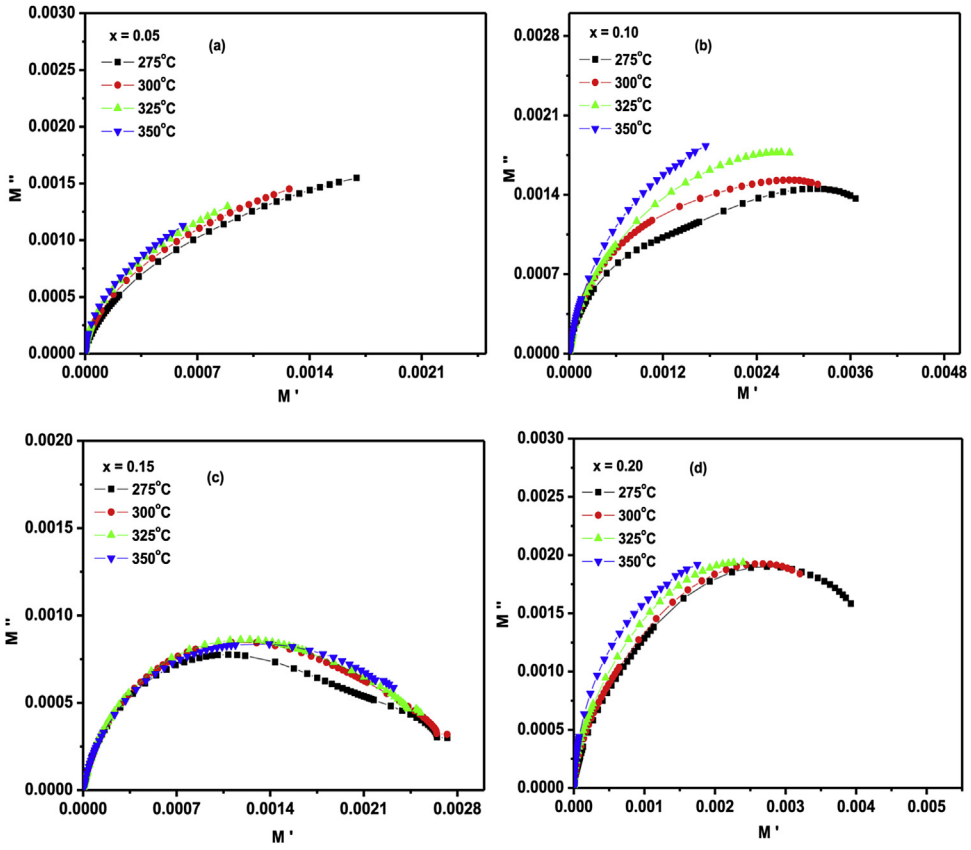

Fig. 7. Complex modulus spectrum (M′ vs M″) of $Bi_4V_{2-x}Sm_xO_{11}$ for x = 0.05, 0.10, 0.15 and 0.20 at different temperatures.

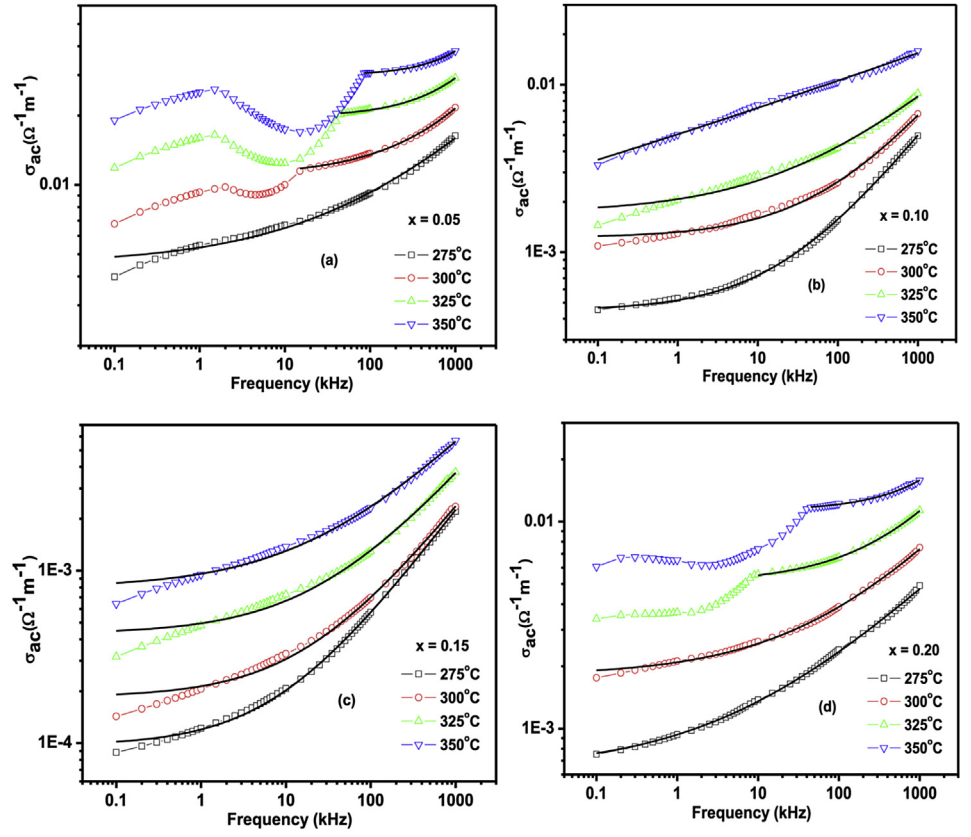

Fig. 8. Variation of ac conductivity with frequency of $Bi_4V_{2-x}Sm_xO_{11}$ for x = 0.05, 0.10, 0.15 and 0.20 at different temperatures.

Table 3
Value of fitting parameters obtained from Jonscher's power law at different temperatures.

	T (°C)	Parameter			Goodness of fit (R^2)
		σ_{dc} (Ω^{-1} m^{-1})	A	n	
x = 0.05	275 °C	0.00454	5.75343×10^{-5}	0.38297	0.99633
	300 °C	0.01097	2.2921×10^{-6}	0.61021	0.99825
	325 °C	0.02999	4.37408×10^{-9}	1.04494	0.99909
	350 °C	0.00454	5.75343×10^{-5}	0.38297	0.99994
x = 0.10	275 °C	0.00044	1.05545×10^{-6}	0.6056	0.99963
	300 °C	0.00122	1.80375×10^{-6}	0.57877	0.9983
	325 °C	0.00171	1.97942×10^{-5}	0.42271	0.99469
	350 °C	0.00047	0.0014	0.17133	0.99655
x = 0.15	275 °C	0.00009	2.54303×10^{-7}	0.65476	0.9998
	300 °C	0.00018	3.84864×10^{-7}	0.62556	0.99921
	325 °C	0.00043	1.27165×10^{-6}	0.56817	0.99813
	350 °C	0.00079	5.50878×10^{-6}	0.49037	0.9983
x = 0.20	275 °C	0.00063	2.22267×10^{-5}	0.37766	0.9989
	300 °C	0.00181	1.47229×10^{-5}	0.42952	0.99929
	325 °C	0.00506	2.29231×10^{-6}	0.57209	0.99959
	350 °C	0.01134	1.33774×10^{-7}	0.75436	0.9961

dependent parameter. It is observed that the value of σ (ω) increases with increase in frequency as well as temperature. The fitting parameters A, n and σ_o are calculated by non-linear fit of the above equation with experimental data (shown in Table 3). The black solid lines are the fitted line. It is clear that the value of the n varies between 0 and 1 ($0 \leq n \leq 1$). This suggests that the electrical conduction in the materials are due to thermally activated process [40,41]. This type behavior also reported by the other studied material [33].

Fig. 9 shows the variation of σ_{dc} (grain) with inverse of absolute temperature (10^3/T) of $Bi_4V_{2-x}Sm_xO_{11}$ with x = 0.05, 0.10, 0.15 and 0.20. The conductivity of the materials was evaluated from the Nyquist plots at selected temperatures. The dc conductivity of the materials were calculated by using the relation $\sigma_{dc}=l/R_gA$, where the symbols have their usual meaning. The dc conductivity increases with rise temperature. It is also observed that the dc conductivity decreases with rise in concentration up to 0.15 and then increases. The activation energies were calculated from using the Arrhenius relation $\sigma_{dc} = \sigma_0 \exp\left(\frac{-E_a}{K_B T}\right)$, where the symbols having their usual meaning. The activation energies were found to be 0.59, 0.93, 0.91 and 0.76 eV of $Bi_4V_{2-x}Sm_xO_{11}$ for x = 0.05, 0.10, 0.15 and 0.20 respectively in the temperature region (275–350 °C). These values suggest that a small amount of energies is required to activate the carriers/electrons for electrical conduction.

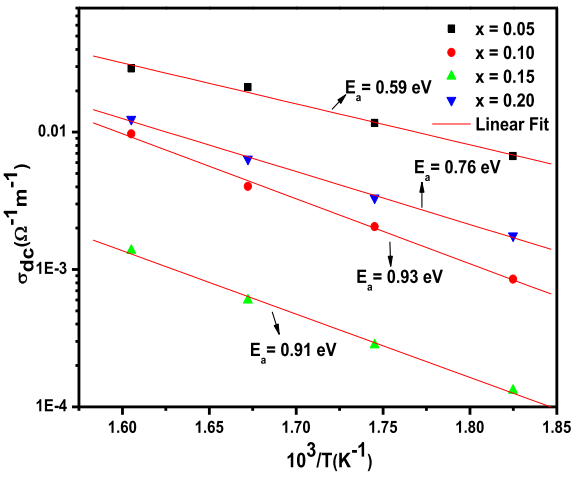

Fig. 9. Variation of dc conductivity with inverse of temperature of $Bi_4V_{2-x}Sm_xO_{11}$ for x = 0.05, 0.10, 0.15 and 0.20.

5. Conclusions

The polycrystalline samples of $Bi_4V_{2-x}Sm_xO_{11}$ with x = 0.05, 0.10, 0.15 and 0.20 were prepared by using solid state reaction technique. Complex impedance spectroscopy was used to characterize the electrical properties of the materials. Both the grain and grain boundary resistance decreases with rise in temperature indicating a typical NTCR behavior of the compounds. Modulus study confirmed the presence of hopping mechanism in the materials. The ac conductivity spectrum was found to obey the Jonscher's universal power law and dc conductivity shows a typical Arrhenius type of electrical conductivity with small amount of energies. The activation energies were found to be 0.59, 0.93, 0.91 and 0.76 eV of $Bi_4V_{2-x}Sm_xO_{11}$ for x = 0.05, 0.10, 0.15 and 0.20 respectively.

Acknowledgments

One of the authors (SB) acknowledges the financial support through RGNF (No. F1-17.1/2012-13/RGNF-2012-13-SC-ORI-25922) to carry out the research work. The authors also acknowledge the financial support through DRS-I of UGC (No. 530/17/DRS/2009), New Delhi, India under SAP and FIST program of DST (No. SR/FST/PSI-179/2012), New Delhi, India for the development of research work in the School of Physics, Sambalpur University, Odisha. One of the authors (BB) acknowledge to the SERB under DST Fast Track Scheme for young Scientist (Project No. SR/FTP/PS-036/2011) New Delhi, India.

References

[1] B. Aurivillius, Mixed bismuth oxides with layered lattices, Arki Kemi 1 (1949) 463–480.
[2] F. Abraham, J.C. Boivin, G. Mairesse, G. Nowogrocki, The bimevox series: a new family of high performances oxides ion conductor, Solid State Ionics 40–41 (1990) 934–937.
[3] A. Cherrak, R. Hubaut, Y. Barbaux, G. Mairresse, Catalytic properties of bismuth vanadates based catalysts in oxidative coupling of methane and oxidative dehydrogenation of propane, Catal. Lett. 15 (1992) 377–383.
[4] G. Pasciak, J. Chmielowiec, P. Bujlo, BIMEVOX materials for application in SOFCS, Mater. Sci. Polond 23 (2005) 209–219.
[5] G. Singla, K. Singh, Dielectric properties of Ti substituted $Bi_{2-x}Ti_xO_{3+x/2}$ ceramics, Ceram. Int. 39 (2013) 1785–1792.
[6] F. Abraham, M.F. Debreuille-Gresse, G. Mairesse, G. Nowogrocki, Phase transitions and ionic conductivity in $Bi_4V_2O_{11}$ an oxide with a layered structure, Solid State Ionics 28–30 (1988) 529–532.
[7] C. Pirovano, M.C. Steil, E. Capoen, G. Nowogrocki, R. Vannier, Impedance study of the microstructure dependence of the electrical properties of BIMEVOXes, Solid State Ionics 176 (2005) 2079–2083.

[8] E.D. Politova, E.A. Fortalnove, G.M. Kaleva, et al., Solid solutions on the base of bismuth vanadate: preparation structure, phase transitions, dielectric and transport properties, Solid State Ionics 192 (2011) 248–251.
[9] M.V. Morozova, E.S. Buyanova, Yu.V. Emelyanova, et al., Specific features in the synthesis, crystal structure and electrical conductivity of BICUTIVOX, Solid State Ionics 201 (2011) 27–34.
[10] N.A. Szreder, P. Kupracz, M. Przesniak-Welenc, et al., Nonlinear and linear impedance of bismuth vanadate ceramics and its relation to structural properties, Solid State Ionics 271 (2015) 86–90.
[11] Sei-Ki Kim, M. Miyayama, Anisotropy in oxide ion conductivity of $Bi_4V_{2-x}Co_xO_{11-\delta}$, Solid State Ionics 104 (1997) 295–302.
[12] S. Gupta, K. Singh, Structural and optical properties of melt quenched barium doped bismuth vanadates, Phys. B 431 (2013) 89–93.
[13] R. Kant, K. Singh, O.P. Pandey, Structural and ionic conductive properties of $Bi_4V_{2-x}Ti_xO_{11-\delta}$ ($0 \le x \le 0.4$) compound, Mater. Sci. Eng. B 158 (2009) 63–68.
[14] E.D. Politova, J.N. Torba, E.A. Fortalnova, et al., Phase transitions and transport properties of the bismuth vanadate-based $(Bi, La)_4$ $(V, Zr)_2$ O_{11-z} ceramics, Acta Phys. Pol. A 117 (2010) 20–23.
[15] J.N. Torba, N.V. Golubko, E.A. Fortalnova, et al., Electroconductive and dielectric properties of composites based on bismuth vanadate, Acta Phys. Pol. A 117 (2010) 24–26.
[16] S. Thakur, M. Devi, K. Singh, Structural and optical properties of La and Gd substituted $Bi_{4-x}M_xV_2O_{11-\delta}$ ($0.1 \le x \le 0.3$), Ionics 20 (2014) 73–81.
[17] S. Gupta, K. Singh, Effect of two different dopants (Mg^{2+} and Ca^{2+}) and processing parameters on γ-phase stabilization and conductivity of $Bi_4V_2O_{11-\delta}$, Ceram. Int. 41 (2015) 9496–9504.
[18] N. Yasudaa, M. Miyayama, T. Kudo, Impedance analysis on electrical anisotropy of layer – structured $Bi_4V_{2(1-x)}Co_{2x}O_{11-\delta}$ single crystals, Mater. Res. Bull. 36 (2001) 323–333.
[19] D.S. Khaerudini, G. Guan, P. Zhang, A. Abudula, Oxide ion conductors based on niobium-doped bismuth vanadate: conductivity and phase transition features, Ionics 22 (2016) 93–97.
[20] S. Beg, N.S. Salami, Study on the electrical properties of Co-Ti double substituted $Bi_4V_2O_{11}$, J. Alloys Compd. 586 (2014) 302–307.
[21] O. Thiabgoh, H. Shen, T. Eggers, A. Galati, S. Jiang, J.S. Liu, Z. Li, J.F. Sun, H. Srikanth, M.H. Phan, Enhanced high-frequency magneto-impedance response of melt-extracted $Co_{69.25}Fe_{4.25}Si_{13}B_{13.5}$ microwires subject to joule annealing, J. Sci. Adv. Mater. Devices 1 (2016) 69–74.
[22] Arcady Zhukov, Ahmed Talaat, Mihail Ipatov, Alexandr Granovsky, Valentina Zhukova, Estimation of the frequency and magnetic field dependence of the skin depth in Co-rich magnetic microwires from GMI experiments, J. Sci. Adv. Mater. Devices 1 (2016) 388–392.
[23] S. Bag, B. Behera, Structural, dielectric and ferroelectric properties of layered bismuth oxide of Sm doped $Bi_4V_{2-x}Sm_xO_{11}$ ceramics, Int. J. Emerg. Technol. Adv. Eng. 5 (2015) 321–326.
[24] S. Beg, Niyazi Al-Areqi, Ahlam S. Al-Alas, Shehla Hafeez, Study on phase stabilization performance of $BiCo_{0.20-x}Ni_xVO_x$ solid electrolyte, Phase Transition 87 (2014) 96–109.
[25] S. Beg, S. Hafeez, Niyazi A.S. Al-Areqi, Influence of calcium substation on the phase transition and ionic conductivity in BICAVOX oxide ion conductor, Phase Transitions 83 (2010) 169–181.
[26] E. Wu, POWD. An Interactive Powder Diffraction Data Interpretation and Indexing Program. Ver 2.2, School Physical Science, Flinders University South Bedford Park, SA 5042, Australia, 1989.
[27] P. Scherrer's, Gottinger Nachr. 2 (1918) 98–100.
[28] J.R. Mac Donald, Impedance Spectroscopy, John Wiley and Sons, New York, 1987.
[29] C.K. Lee, C.S. Ong, Synthesis and characterization of rare earth substituted bismuth vanadate solid electrolytes, Solid State Ionics 117 (1999) 301–310.
[30] B. Behera, P. Nayak, R.N.P. Choudhary, Structural, dielectric and impedance properties of $NaCa_2V_5O_{15}$, Curr. Appl. Phys. 9 (2009) 201–205.
[31] V. Provenzano, L.P. Boesch, V. Volterra, C.T. Moynihan, P.B. Macedo, Electrical Relaxation in $Na_2O.3SiO_2$ glass, J. Am. Ceram. Soc. 55 (1972) 492–496.
[32] H. Jain, C.H. Hsieh, Window effect in the analysis of frequency dependence of ionic conductivity, J. Non-Crystall. Solids 172–174 (1994) 1408–1412.
[33] S. Gupta, K. Singh, Dielectric, optical and structural properties of $Bi_4V_{2-x}Sr_xO_{11-\delta}$ ($0.05 \le x \le 0.20$), J. Phys. Chem. Solids 85 (2015) 18–25.
[34] H. Singh, A. Kumar, K.L. Yadav, Structural, dielectric, magnetic, magnetodielectric and impedance spectroscopic studies of multiferroic $BiFeO_3$–$BaTiO_3$ ceramics, Mater. Sci. Eng. B 176 (2011) 540–547.
[35] B. Behera, P. Nayak, R.N.P. Choudhary, Studied of dielectric and impedance properties of $KCa_2V_5O_{15}$ ceramics, J. Phys. Chem. Solids 69 (2008) 1990–1995.
[36] B. Behera, P. Nayak, R.N.P. Choudhary, Study of complex impedance spectroscopic properties of $LiBa_2Nb_5O_{15}$ ceramics, Mater. Chem. Phys. 106 (2007) 193–197.
[37] F. Borsa, D.R. Torgeson, S.W. Martin, H.K. Patel, Relaxation and fluctuations in glassy fast-ion conductors: wide-frequency-range NMR and conductivity measurement, Phys. Rev. B 46 (1992) 795–800.
[38] P.R. Das, B. Pati, B.C. Sutar, R.N.P. Choudhury, Electrical properties of complex tungsten bronze ferroelectrics; $Na_2Pb_2R_2W_2Ti_4Nb_4O_{30}$ (R = Gd, Eu), Adv. Mater. Lett. 3 (2012) 8–14.
[39] A.K. Jonscher, The 'universal' dielectric response, Nature 267 (1977) 673–679.
[40] N.K. Mohanty, R.N. Pradhan, S.K. Satpathy, et al., Electrical transport properties of layered structure bismuth oxide: $Ba_{0.5}Sr_{0.5}Bi_2V_2O_9$, J. Mater. Sci. Mater. Electron. 25 (2014) 117–123.
[41] P. Khatri, B. Behera, V. Srinivas, R.N.P. Choudhary, Structural and dielectric properties of $Ba_3V_2O_8$ ceramics, Curr. Appl. Phys. 9 (2009) 515–519.